

Design of wave-optical structured substrates for ultra-thin perovskite solar cells

Sirazul Haque*, Miguel Alexandre, Manuel J. Mendes*, Hugo Águas, Elvira Fortunato, Rodrigo Martins

i3N/CENIMAT, Department of Materials Science, Faculty of Science and Technology, Universidade NOVA de Lisboa and CEMOP/UNINOVA, Campus de Caparica, 2829-516 Caparica, Portugal

**Corresponding authors: s.haque@campus.fct.unl.pt, mj.mendes@fct.unl.pt*

Abstract

Photonic micro/nano-structures in the wave-optics regime have shown to be a promising strategy for effective broadband light capture in ultra-thin devices, opening a window of opportunity for cheap, efficient, lightweight and flexible photovoltaics (PV). Here we design, from an optical standpoint, a novel industrially-attractive concept where light trapping is obtained by conformably depositing the solar cell materials onto previously-patterned photonic substrates. This solution is applied and optimized for perovskite solar cells (PSCs) with distinct thicknesses of the perovskite absorber - the conventional (500 nm) and ultra-thin (300 nm) in view of enhanced flexibility - yielding photocurrent improvements up to 22.8% in superstrate cell configuration and 24.4% in substrate-type configuration; thereby coming relatively close to the fundamental Lambertian limits. Furthermore, these structures also show an omni-direction optical response for incidence angles up to 70° for all cases, therefore demonstrating the viability of this light trapping method for implementation in flexible PV devices operating under bending. The photonic-enhanced ultra-thin solar cells designed here ultimately support the reduction of material usage in PSC technology, which is especially beneficial to mitigate lead usage, without impacting the device's performance.

Keywords: Photovoltaics, Photonics, Perovskite Solar Cells, Light Trapping, Flexibility and Photocurrent Enhancement

1. Introduction

Light trapping using periodic arrays of nanostructures has proven to be an effective method to solve the well-known dichotomy where thicker solar cells are optically favorable and electrically disadvantageous, and conversely for thinner devices, ultimately opening a new window of research possibilities pointing to cost-competitive photovoltaics (PV)[1–4]. This method relies on improved anti-reflection and light scattering effects, that can be optimized to significantly enhance broadband light absorption in ultra-thin absorber layers, thereby increasing their efficiency[5,6]. This reduction in solar cells thickness also enables several advantages, be it in electronic properties such as open circuit voltage and carrier collection, or even in other properties like cells' stability and mitigation of hazardous/toxic compounds (e.g. Pb) for the case of perovskite[5,7–12]. Furthermore, it also creates a conducive scenario to improve the performance of ultra-thin and low-cost solar cells for portable electronic devices with higher intrinsic mechanical flexibility[5,6,8,13,14].

Equivalently, organic–inorganic halide perovskite semiconductors have been extensively researched during the last decade due to their impressive optoelectronic properties[5]. Perovskite solar cells (PSCs) are a promising step in the recent evolution of PV due to their high light absorption coefficient[15], tunable band structure[16,17], high charge carrier mobility[18,19], and low fabrication cost[20]. Based on the aforementioned characteristics conjoined with deeper understanding of materials and device properties, brought out by the vast research in the area of materials science, PSCs efficiency saw a rapid improvement, having grown from ~3.8% in 2009 to > 24.2% in 2019[21–26]. However, the progress in PSC technology hitherto has been mainly achieved by optimizing the process techniques of the perovskite layer and the quality of the cells' interfaces[20,27–29].

Nevertheless, keeping a balance between generating and collecting carriers in PSCs still remains a major challenge to overcome. In conventional PSCs, a perovskite layer with typically ~500 nm thickness is required to allow sufficient light absorption (hence, photocarrier generation) and maximize efficiency. In contrast, thinner absorber layers can reduce bulk recombination and facilitate carrier collection at the contacts[30]. Concomitantly, the use of less amount of absorber material is also an important mean to mitigate the usage of toxic Pb in the perovskite[7]. However, reducing the absorber thickness comes at the expense of increasing the optical losses in PSCs; particularly for the longer sunlight wavelengths in the VIS-NIR range that require a large travel path inside the absorber to generate photocurrent. Therefore, effective light trapping (LT) strategies are crucial to improve performance in ultra-thin solar cells, ultimately enabling highly efficient and flexibility PSCs[5,6].

While silicon-based solar cells have been extensively tested regarding the implementation of advanced LT schemes, their application in PSCs is still in its infancy. This lethargy in LT adoption comes, understandably, from the high absorption properties of these perovskite materials. Regardless, for ultra-thin technology LT methodologies become viable to mitigate non-absorption losses[5,6,31]. Different LT approaches have been proposed in the last few years for PSCs, such as micro lens or nanocone arrays[32–34], random pyramids[35], fiber array-based anti-reflection front electrodes[36], nanophotonic front[37] and back electrodes[11], nanophotonic perovskite layers[7], nano- and micro-patterned charge transport layers[38,39], and corrugated substrates for single[40] and multijunction[41–43] PSCs, as well as the exploitation of surface plasmon resonances, e.g.: plasmonic nanoparticles[44–46] and light grating-coupled plasmons[46]. Nonetheless, most of these approaches have yet to demonstrate pronounced absorption improvements that justify the efforts in their integration, or have even caused electrical deterioration of the devices.

In earlier theoretical contributions[3,5,6], novel LT designs operating in the wave-optics regime were shown to allow pronounced photocurrent gains in thin-film solar cells via the incorporation of wavelength-sized pyramidal-like features in the front contact of PV devices with a substrate configuration. This enabled the demonstration of LT levels approaching the ideal Lambertian limits of geometric optics. However, the implementation of such LT architecture may be difficult to realize in practice, since the photonic elements need to be patterned on top of the planar cell layers, during the final processing stages, which may cause the degradation of the delicate materials of the devices during the micro-patterning fabrication[31,47].

In this work, an unprecedented wave-optical solution was explored for PSC application, via the optimization of photonic-structured substrates supporting the cells. By micro-patterning the substrates with wavelength-sized semi-spheroidal features, it is possible to achieve high-performing LT-enhanced PSCs due to the conformal deposition of the cells' materials onto the photonic substrates. Such innovative industrially-attractive LT design is studied and optimized here for two different solar cell configurations: superstrate and substrate; considering distinct perovskite absorber thicknesses (300 and 500 nm), as sketched in Fig. 1. This approach has significant practical benefits regarding its applicability, when compared with post-patterned photonic structures implemented on the ETLs, since here the PSC layers are wet-coated by usual methods over a substrate already patterned with LT structures, hence making the photonic integration independent of the PSC's fabrication. This is particularly beneficial in order to prevent the LT implementation from deteriorating not only the PSC layers but also less robust polymeric substrates used in flexible devices[13,48]. Besides, this enables the widespread application of the micro-structured substrates as generic photonic platforms to support other types of thin-film PV

devices (based in Si[6], CIGS[49], CZTS[50], organic[13], tandems[51] etc.), after straightforward adaptation/tuning of the geometrical parameters of the LT structures.

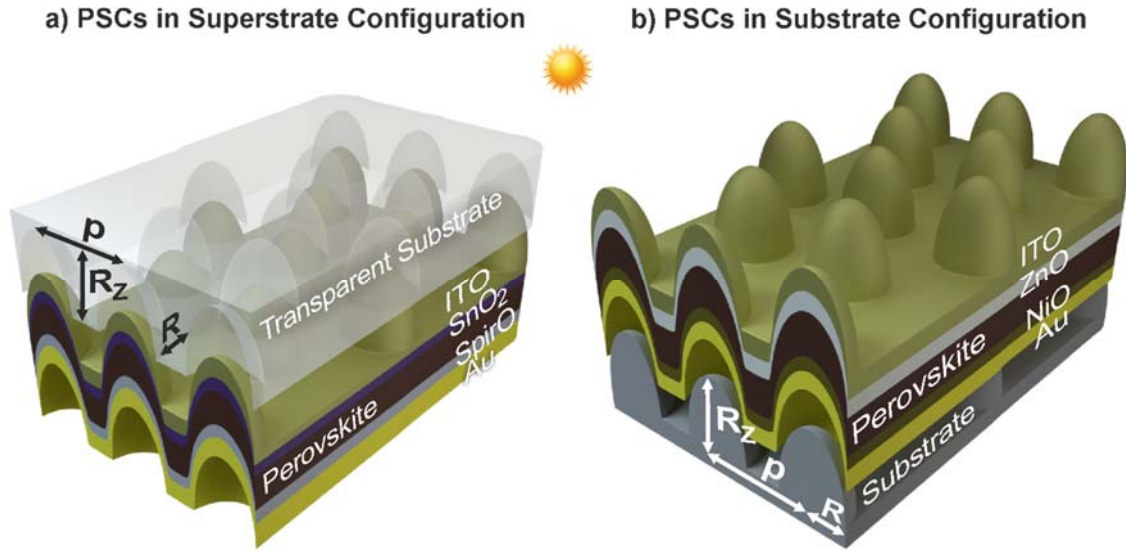


Fig. 1: Two types of photonic-patterned substrates were studied and optimized for two types of PSC architectures: the conventional superstrate configuration (a), compatible only with transparent substrates (e.g. flexible polymers as PEN/PET)[48,52]; and the so-called “inverted” substrate configuration (b) enabling a larger variety of substrates (e.g. flexible opaque materials as metal sheets)[52–54]. The LT structures patterned on the substrates are modelled as a hexagonal array (with pitch p) of vertically-aligned semi-prolate features with radii R and R_z , respectively along the in-plane direction and illumination axis. The PSC layers are conformally deposited over such spheroidal features: **a)** superstrate-type layer configuration, in which light comes into the devices from the substrate side, composed of transparent conducting oxide (TCO, made of ITO)/electron transport layer (ETL, made of SnO_2)/perovskite absorber (methylammonium lead iodide, $\text{CH}_3\text{NH}_3\text{PbI}_3$)/hole transport layer (HTL, made of Spiro-OMeTAD)/rear metal contact (made of gold, Au); **b)** substrate-type layer configuration, in which light comes into the devices from the films’ side, composed of TCO (made of ITO)/ETL (made of ZnO)/perovskite ($\text{CH}_3\text{NH}_3\text{PbI}_3$)/HTL (made of NiO_x)/rear contact (Au).

Previous work has shown that hexagonal arrays of high-index semi-spheroidal features patterned on the cells’ illuminated front surface allow pronounced broadband absorption enhancement in the PV absorber of thin-film solar cells[5,6,31,47]. Here, such type of features is produced in the cells’ front due to the conformal deposition of the PSC layers over the patterned substrates (see Fig. 1). Apart from allowing higher optical density with thinner absorber thickness, the LT geometries investigated here provide three other practical advantages: 1) the “round” spheroidal-type shapes can avoid losses associated with nanostructures having high spatial curvatures or

sharp edges[2,55]; 2) arrays of such semi-spheroidal features can be easily fabricated by industrially-attractive patterning methods such as colloidal lithography - a low cost soft-lithography process capable of engineering with nano/micrometer resolution with high uniformity throughout large areas[31,47]; 3) the inherent wide angular acceptance of this type of structures is particularly important for flexible solar cells[6,55], since their operation under bending implies the simultaneous conversion of light coming from a broad angular range.

2. Modelling Method

We employed a 3D finite difference time domain (FDTD) numerical method to rigorously model optical effects in the photonic-structured PSCs[3,5,6,56]. This method is regarded as a preferential approach for solving electromagnetic problems in the wave-optics regime, especially for light management in solar cells, mainly owing to its conceptual simplicity and versatility[3]. Furthermore, its capability for single-run broadband simulations is of particular interest for application in photovoltaics[2,5,6]. The two different PSC architectures of Fig. 1 were modelled, in which the solar cells are composed of 5 layers conformally coated onto micro-structured substrates. The optical response of the materials is determined by their complex refractive index ($N=n+ik$) spectra, which were taken from published experimental data and are plotted in section S1 of Supplementary Material (SM). The perovskite absorber material considered in this work is methylammonium lead iodide, MAPbI_3 , taking a widely-used refractive index function fitted from measured values provided by Phillips *et al.*[57], available in a common database[58]. However, it should be pointed out that, contrarily to other more matured PV technologies, PSCs are still highly dependent on the specific fabrication conditions and process materials used. Therefore, there is presently no (n, k) dataset that can be taken as technological standard. In view of that, for comparison the main computations presented here were recalculated considering a different measured refractive index provided by Eerden *et al.*[59], whose results are presented in section S6 of SM. For the superstrate configuration (Fig. 1a), the refractive index of the transparent substrate was accounted for by a fixed real value, attributed to the background index of the simulation volume, equal to $n=1.5$ (e.g. similar to the index of PET)[58]. For the substrate configuration (Fig. 1b), a background index $n=1.6$ was taken in order to account for a typical transparent adhesive material used for encapsulation over the PSC layers[58].

The photonic features on the substrates are arranged in a hexagonal array, thus mimicking the structures patterned by colloidal soft-lithography[31,47]. Further details regarding the simulation setup in the FDTD programs can be found in section S2 of SM. We are interested in analyzing the light absorption along the PSC structures of Fig. 1, i.e. the power absorbed per unit volume

(P_{ABS}) in each element of the structures which is given by the resulting electric field distribution established in its material:

$$P_{ABS} = \frac{1}{2} \omega \varepsilon'' |\mathbf{E}|^2 \quad (1)$$

where $|\mathbf{E}|^2$ is the electric field intensity, ω is the angular frequency of the light and ε'' is the imaginary part of the dielectric permittivity. P_{ABS} is normalized by the source power to obtain the absorption density (p_{ABS} , units of m^{-3}). The absorption of light for a particular wavelength (λ) is determined by integrating p_{ABS} along the absorber volume: $Abs(\lambda) = \int p_{ABS}(\lambda) dV$. The number of photons absorbed per unit volume and per unit time is the photon absorption rate: $g(\omega) = P_{ABS}/E_{PH}$, where $E_{PH} = \hbar\omega$ is the photon energy. Here we consider that each absorbed photon excites one electron-hole pair, so g is equivalent to the optical generation rate. Since the illumination is provided by a broadband source, characterized by a spectral irradiance (instead of a power density), the E-field is substituted by an electric-field spectral density such that its intensity, $|\mathbf{E}|^2$, becomes with units of $\text{V}^2\text{m}^{-2}\text{Hz}^{-1}$. In this way, g is normalized to a spectral generation rate (in units of $\text{m}^{-3}\text{s}^{-1}\text{Hz}^{-1}$) such that the total generation rate (G , units of $\text{m}^{-3}\text{s}^{-1}$) is determined by integrating over the frequency range of the source bandwidth: $G = \int g(\omega) d\omega$ [60].

The wavelength range of the illumination source was 300-1000 nm in all calculations, since it corresponds to the most significant portion of the photocurrent spectrum of PSCs [5]. In this study, we considered an ideal internal quantum efficiency of the PSCs equal to 100% (i.e. every photon absorbed in the perovskite material generates carriers collected by the contacts), since we are mainly concerned with the optical rather than the electrical transport behavior of the cells [3,5,6]. Thus, the photocurrent density (J_{PH}) is determined by integrating the absorption in the perovskite material, multiplied with the solar power spectrum AM1.5G ($I_{AM1.5}$, units of $\text{Wm}^{-2}\text{m}^{-1}$), along the chosen computation wavelength range (300-1000 nm):

$$J_{PH} = e \int \frac{\lambda}{hc} Abs(\lambda) I_{AM1.5}(\lambda) d\lambda \quad (2)$$

where e is the electron's charge, h is Planck's constant and c is the light velocity in vacuum. This spectrally-integrated J_{PH} creates an upper-limit to the attainable short-circuit current density of the cell, since it neglects any electrical losses. Furthermore, this parameter will also be used in the simulations as the figure-of-merit to optimize the geometry of the substrate features - modelled as semi-spheroidal shapes with an axis of revolution aligned with the illumination direction.

A particle swarm optimization algorithm (PSO) [6,60] was employed in the FDTD programs to find the optimized set of parameters for the semi-spheroidal structures of the photonic substrates. Population-based stochastic optimization methods, such as PSO, are the most favorable approach to perform the complete screening of complex physical systems with a strong correlation between a high numbers of parameters, as in the present wave-optics regime, in order to determine

precisely the global maximum of any given figure-of-merit. Further details concerning the PSO methodology are given in section S2 of SM and in previous contributions[3,6,61].

3. Optimized photonic-structured perovskite solar cells

In this section we present the results of the optimized LT structures considering both configurations depicted in Fig. 1. The superstrate configuration (Fig. 1a) is the current record efficiency holder in PSCs[26]. Nevertheless, the requirement for superstrate solar cells to be supported on transparent substrates is a major limiting factor if one is to achieve ultra-thin and flexible devices. This can be mostly attributed to the proclivity for low degradation temperatures, usually seen in bendable transparent materials (e.g. PEN, PET), that severely restricts the PSCs fabrication conditions[52]. Subsequently, there has been a shifting interest to the substrate configuration (Fig. 1b), since it allows for a more versatile gamut of materials to be used, such as the case of opaque and much more robust bendable materials (e.g. metal foils, PI)[52–54]. Besides, the substrate-type PSC structure is compatible with its application as sub-cell in monolithic tandem devices (e.g. perovskite top cells coupled with Si[51] or CIGS[52] bottom cells), which is another research line attracting much interest lately.

The materials considered for the PSCs' layer structure are based on state-of-the-art devices produced with low-temperature (< 200 °C) fabrication, to allow compatibility with polymeric flexible substrates. Different materials are considered for the ETL and HTL in each configuration: SnO_2 and ZnO are the materials taken for the ETLs, and Spiro-OMeTAD and NiO are those of the HTLs, respectively in the superstrate and substrate configuration. Apart from their low-temperature processing, both ETL materials have recently been revealing better stability and performance than the conventional TiO_2 [26,62,63]. As for the HTLs, Spiro is the material that has allowed the highest efficiencies so far. However, due to its high cost, other HTLs have been investigated, being NiO -based materials those that appear to be the best alternative, especially for flexible applications that can particularly benefit from low-cost devices[64]. The conventional MAPI (methylammonium lead iodide) perovskite was taken for the absorber material, with two different thicknesses analyzed in this work: the standard 500 nm and a thinner 300 nm layer.

Table 1 shows the sets of relevant physical parameters optimized for the aforementioned cell designs, where R , R_z and p define the geometry of the LT features patterned on the substrates (see Fig. 1) and the values t_{layer} correspond to the thickness of specific flat layers. These quantities were taken as variables by the PSO algorithm that iteratively searched for the best set of parameters that maximizes the photocurrent (J_{PH} , equation 2) produced in the perovskite material. Row 1 of Table 1 shows the *Lambertian* limits of geometrical optics for the analyzed perovskite absorber layers, as described in an earlier contribution of the authors[5]. In this case, the values

of the LT enhancement were calculated relative to a cell without LT in the same regime of geometrical optics. Row 2 and 4 present the optically-optimized values for the thicknesses of the front contact of planar PSCs, which provides an anti-reflection coating (ARC) effect, and of the HTLs, respectively for superstrate and substrate configuration. These serve as reference results for comparison with the ones obtained with the photonic semi-spheroidal structures shown in rows 3 and 5, respectively. The results and discussion for the two optimized types of planar PSCs are presented in sections S3 and S4 of SM.

Table 1: Highest J_{PH} values obtained for the optimized LT structures for two distinct PSCs, with 300 or 500 nm perovskite layer thicknesses, in two different solar cells configurations, superstrate and substrate-type, considered in this work. The geometrical optimization parameters (R , R_z , p , t_{ITO} , t_{SnO_2} , t_{Spiro}) and (R , R_z , p , t_{ITO} , t_{ZnO} , t_{NiO}), for the LT structures in superstrate and substrate configurations, respectively, are sketched in Fig. 1. The results are compared with the reference cases of planar PSCs having optically-optimized TCO/ETL and HTL thicknesses, as well as with the theoretical limits in the regime of geometrical optics attainable with a *Lambertian* scattering front surface.

Light Trapping Structures	Absorber: 300 nm Perovskite layer		Absorber: 500 nm Perovskite layer		Row index
	Optimal Parameters	J_{PH} , mA/cm ² (LT enhancement)	Optimal Parameters	J_{PH} , mA/cm ² (LT enhancement)	
<i>Lambertian</i> surface	-	33.8 (28.0%)	-	35.3 (25.0%)	1
Optimized Planar PSCs in Superstrate Configuration (Fig. S3)	$t_{ITO} = 50$ nm $t_{SnO_2} = 25$ nm $t_{Spiro} = 50$ nm	25.0	$t_{ITO} = 50$ nm $t_{SnO_2} = 25$ nm $t_{Spiro} = 50$ nm	27.1	2
Optimized Photonic PSCs in Superstrate Configuration (Fig. 2)	$t_{ITO} = 50$ nm $t_{SnO_2} = 25$ nm $t_{Spiro} = 50$ nm $R = 219.2$ nm $R_z = 167.6$ nm $p = 558.6$ nm	30.7 (22.8%)	$t_{ITO} = 50$ nm $t_{SnO_2} = 25$ nm $t_{Spiro} = 50$ nm $R = 206.2$ nm $R_z = 259.8$ nm $p = 508.1$ nm	32.5 (20.0%)	3
Optimized Planar PSCs in Substrate Configuration (Fig. S5)	$t_{ITO} = 50$ nm $t_{ZnO} = 100$ nm $t_{NiO} = 10$ nm	22.5	$t_{ITO} = 50$ nm $t_{ZnO} = 100$ nm $t_{NiO} = 10$ nm	25.1	4
Optimized Photonic PSCs in Substrate Configuration (Fig. 3)	$t_{ITO} = 50$ nm $t_{ZnO} = 100$ nm $t_{NiO} = 10.1$ nm $R = 239.0$ nm $R_z = 309.2$ nm $p = 480.1$ nm	28.0 (24.4%)	$t_{ITO} = 50$ nm $t_{ZnO} = 100$ nm $t_{NiO} = 11.1$ nm $R = 200.2$ nm $R_z = 519.3$ nm $p = 484.4$ nm	30.2 (20.3%)	5

The PSO “smart search” was constrained to certain parameters’ boundaries that were set based on reasonable values for their domains. Several optimization runs were performed with different initial parameter sets spanning the domain space, and it was found that the algorithm consistently converged to thicknesses of the selective contact layers (t_{ITO} , t_{SnO_2} , t_{Spiro} , t_{ZnO} , t_{NiO}) at the minimum allowed value of the domain, defined in order to guarantee their electrical performance. Therefore, it is clear that such layers are optically undesirable, but their presence is electrically needed with a minimum thickness to guarantee effective current extraction[65,66]. The variation of photocurrent with the thickness of such contact layers is analyzed in sections S3 and S4 of SM. As the main goal here is the investigation of an optical scheme yielding the maximum degree of light trapping in PSCs, the present study considered optically-favorable values for such layer thicknesses indicated in Table 1, corresponding to the minimum values within the defined “electrical limits” marked in Figs. S2 and S4 in SM. As can be observed these figures, different thicknesses would lead to slight deviations in the optimized parameters and resulting J_{PH} maxima, but would not imply significant differences in the overall trends and discussion given here[3,5,6].

3.1 Photonic-enhanced PSCs in superstrate configuration

We begin by analyzing the results obtained with the optimized set of geometrical parameters of PSCs in superstrate configuration (depicted in Fig. 1a), which are presented in Fig. 2. The absorption spectra of the optimized LT structures (corresponding to row 3 of Table 1) are compared to those of the planar reference cells (row 2 of Table 1) in Fig. 2a,b, for the perovskite absorber thicknesses (300 and 500 nm) considered in this study. Figs. 2c,d show the p_{ABS} profiles of PSCs with LT structures, along the xz plane passing by the center of a semi-spheroidal feature, for four different wavelengths along the illumination spectrum.

Looking at the reference planar cells (blue curves in Fig. 2a,b), both 300 and 500 nm cells show a similar broadband behavior, with the 300 nm cell presenting an overall lower absorption, from the shorter light travel path in the absorber. The considerably high absorption in the perovskite active region (mainly corresponding to the 450-750 nm wavelength range in Fig. 2) evidences well the outstanding perovskite optical properties, preceded by a small absorption drop in the UV-blue range (300-450 nm) due to reflection and parasitic absorption in the front contact (ITO and SnO_2 layers). This drop is slightly lower (~5%) for the 300 nm thick cell. In the near-infrared (NIR) there is a more abrupt absorption drop above 750 nm (nearing 86% and 89% for the 500 and 300 nm thickness, respectively) that coincides with the ~1.5 eV bandgap of the perovskite absorber. Regarding the photonic LT structures (red curves in Fig. 2a,b), there is a pronouncedly higher broadband absorption occurring in the perovskite, brought out by the superior light management scenario created by the photonic features, as explained below.

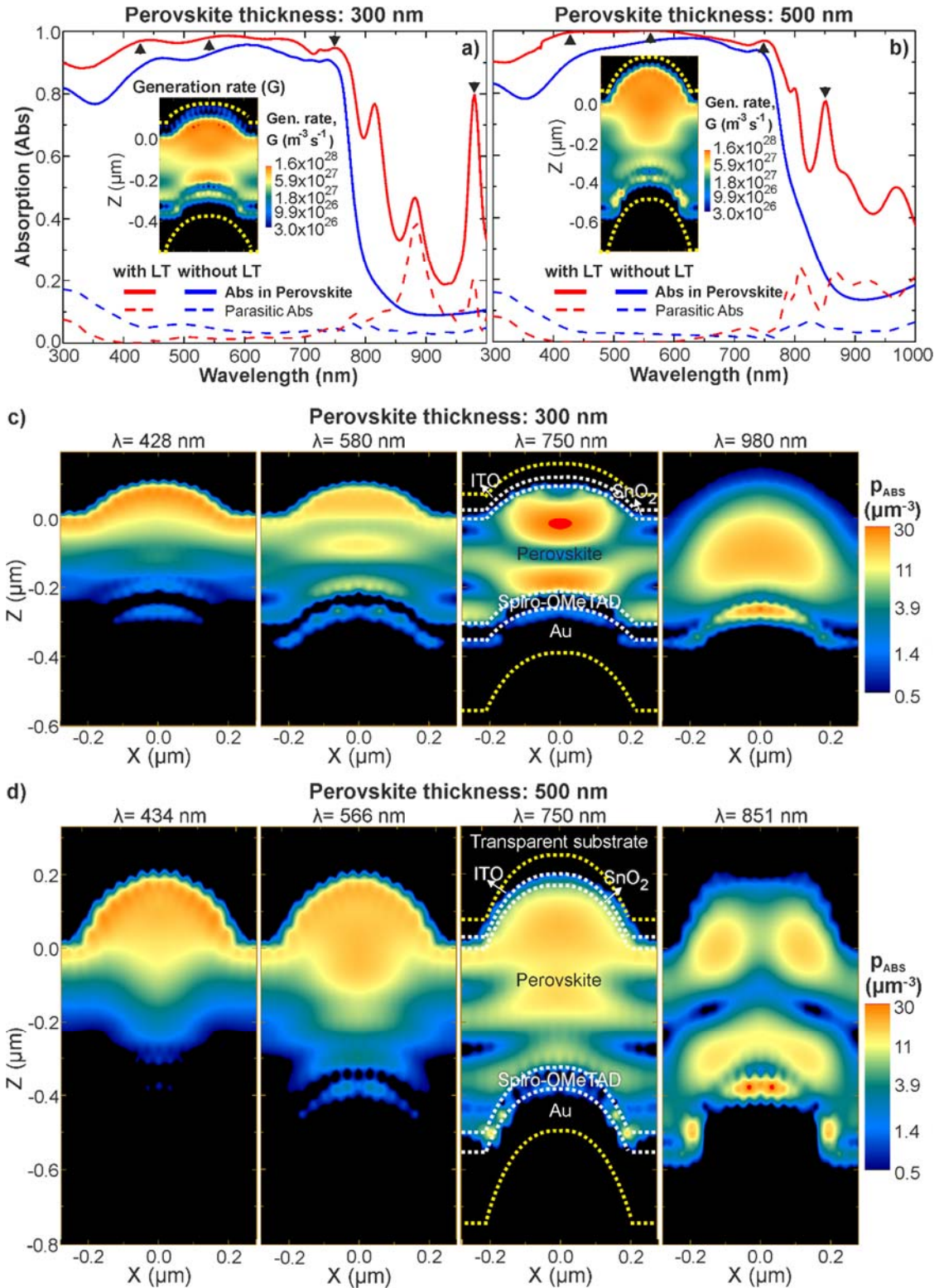


Fig. 2: a,b) Absorption spectra obtained with the optimized LT structures sketched in Fig. 1a, for PSCs in superstrate configuration (red lines, row 3 of Table 1), compared the reference cases of optically-optimized planar cells (blue lines, row 3), for perovskite layers with distinct thickness: a) 300 nm and b) 500 nm. Each graph presents the absorption occurring in the perovskite (solid lines) and the parasitic absorption in the other materials (dashed lines). The inset profiles represent the log-scale distribution of the corresponding

total generation rate, G , along the xz cross-sectional plane of the structures passing by the semi-spheroidal center. **c,d**) Log-scale distributions of the absorption density, p_{ABS} , along the same xz plane of the structures, at the wavelengths of the peaks marked by the arrows in a) and b), respectively for the PSCs with the 300 nm (c) and 500 nm (d) thick perovskite absorbers in superstrate configuration.

The results of Fig. 2 demonstrate a key optical advantage of using photonic-structured PSCs via conformal deposition over patterned substrates: the fact that it is the higher-index perovskite material that plays the main role in anti-reflection and light scattering, which causes the notable absorption gains and extremely low parasitic absorption (even lower than the reference planar cells) in most of the spectrum. The inset images of Fig. 2a,b show the cross section of the solar-spectrum-weighted generation rate (G) along the PSCs with the optimized LT structures, computed over the 300-1000 nm wavelength range. It is notable from these inset profiles that the spectral-integrated absorption occurs primarily in the perovskite. However, Spiro-OMeTAD and Au also show some parasitic contribution, complementarily evidenced in the absorption density profiles (Fig. 2 c,d), especially for longer NIR wavelengths.

The absorption gains in the UV-VIS are attributed to a better light coupling towards the perovskite material by the semi-spheroidal LT features, as a consequence of two optical mechanisms: 1) superior anti-reflection owing to the geometrical index matching[5,6] caused by the curvature of the front layers (ITO, SnO₂ and perovskite) coupled with the propinquity amongst the real part (n) of the refractive indices of ITO, SnO₂ and perovskite (plotted in section S1 of SM). 2) Near-field forward-scattering[5,6] due to the micro-lens effect of the curvature of these three layers, which causes the focal regions of intense electric-field in the top portion of the perovskite observed in the G profiles of Fig. 2a,b and in the p_{ABS} profiles of Fig. 2c,d (mainly for the indicated wavelengths of 580 nm and 566 nm, respectively). It should be noted that the absorption enhancement observed in this spectral range (<750 nm) cannot be due to the rear contact pattern, as the light is strongly absorbed before reaching the back.

In the NIR range, the remarkable absorption increase is chiefly due to the far-field forward scattering caused by the semi-spheroidal shape of both the front and rear features of the PSCs structure, which is favoured by the high real part (n) of the perovskite refractive index. This effect manipulates the vertically-impinging light and redirects it to paths closer to the horizontal plane, thereby leading to optical path length amplification within the cell and coupling with waveguided modes. This is evidenced by the “hot-spots” observed in the p_{ABS} profiles for wavelengths >700 nm, which result from constructive interference between the light waves traveling along the incidence direction and the scattered light that travels along the plane of the cell layers suffering multiple reflections from the top and bottom surfaces of the cell. In this longer wavelength region, the sharp absorption peaks observed in Fig. 2a,b are mainly attributed to guided-mode resonances,

as supported by related studies of LT-enhanced thin-film PV[2,3,5,6,67]. Such resonances were observed to be mostly sensitive to the variation of the in-plane dimension (radius R) and center-to-center distance (pitch, p) of the photonic elements. This is due to the fact that R is the chief parameter determining their scattering cross sections; while p establishes the periodicity and, thus, determines the trapping of waveguided modes in this spectral range[3,5,6]. Results on the LT sensitivity to variations in the geometrical parameters of the photonic structures are presented in Section 5 (Fig. 6).

Concerning the parasitic absorption, below 500 nm wavelengths it mainly occurs within the front ITO and SnO₂, as evidenced by the p_{ABS} plots of Fig. 2c,d. For longer wavelengths it is mostly relegated to the cell's rear contact (Spiro-OMeTAD/Au), with also some contribution from SnO₂ as evidenced by its increasing imaginary part (k) of the refractive index in the NIR (see Fig. S1b in SM). The p_{ABS} plots for >500 nm wavelengths illustrate well this effect. It should also be noted that, throughout the UV-VIS range, the photonic-structured devices show significantly lower absorption losses when compared with the reference ones. This is mostly due to the geometrical index matching caused by the front curvature of the perovskite absorber, which provides a better coupling of light towards such material with high n , preventing its back-reflection towards the ITO/SnO₂ top layers. Nevertheless, in the NIR range (750-1000 nm wavelengths) the parasitic absorption is notably higher with LT structures due to the plasmonic effect caused by the corrugated Au metal layer[2], as seen in the G and p_{ABS} profiles of Fig. 2, which does not occur in the flat metal present in the reference cells (see Figs. S3 and S5 and related discussion in SM). The periodic corrugations of the metallic layer lead to surface plasmon-polariton modes [2] that are confined in a near-field vicinity of the metal-HTL interface, so they mainly lead to enhanced parasitic light absorption within such rear contact. This is supported by the fact that, in the wavelength range (above ~700 nm) where the HTL and rear metal play a pronounced optical role, similar parasitic absorption is observed with the two different perovskite absorber properties considered by the aforementioned distinct refractive index functions of Phillips *et al.*[57] (used in main study, Fig. 2,3) and Eerden *et al.*[59] (compared in SM, Fig. S8).

Comparing this LT design to that of additional thick photonic structures coated on top of the solar cell, as analyzed in a previous study[5], the present implementation bypasses the parasitic absorption within such thick structures, especially for shorter wavelengths. This is because of two reasons: first, the optimized thicknesses of the structured front layers of ITO (50 nm) and SnO₂ (25 nm) are relatively small and the same as the reference cells, thence the parasitic absorption in these materials is quite low; and second, the perovskite is the main scattering material benefiting from an extremely high absorption coefficient (k values) in this range, which also helps mitigate parasitic absorption.

3.2 Photonic-enhanced PSCs in substrate configuration

In this section, we analyze the results obtained with the optimized set of geometrical parameters of PSCs in substrate configuration (Fig. 1b), which are presented in Fig. 3 (corresponding to rows 4 and 5 of Table 1). The absorption profiles of Figs. 2 and 3 show a similar overall optical behavior, despite the difference in cell architecture. However, the light confinement (focusing) in the front curvatures of the perovskite is more intense for the substrate-configuration PSCs, as seen by the higher values of the generation profiles (Fig. 3a,b, insets) and of the p_{ABS} profiles (Fig. 3c,d) at the first two wavelengths, due to the more elongated shape (higher R_Z) of these optimized features relative to those of the superstrate PSCs (see Table 1), for both 300 and 500 nm absorber thicknesses. A bigger height (R_Z) is needed in the substrate configuration to provide a higher effective geometrical index matching for stronger broadband anti-reflection in the UV-VIS range, since this configuration suffers from reduced absorption throughout the 300-700 nm wavelength range, relative to the superstrate configuration, as seen in the absorption spectra of the planar reference cells. At the same time, the structures must maintain a large scattering cross-section for path length amplification in the NIR, so the optimized lateral radii (R) are similar in the superstrate and substrate configuration.

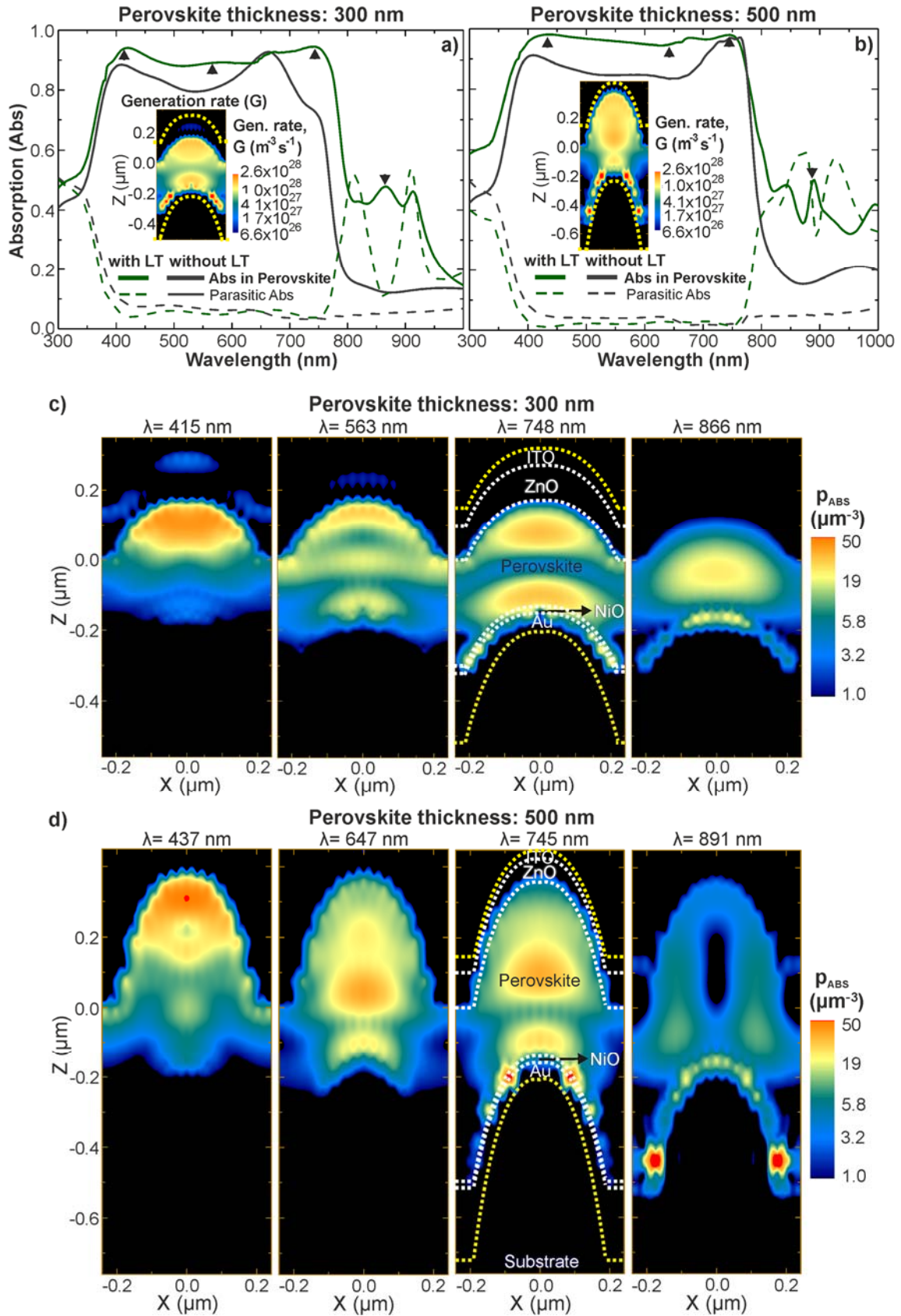


Fig. 3: Similar to Fig. 2 but for the PSCs in substrate configuration sketched in Fig. 1b. **a,b)** Absorption spectra obtained with the optimized LT structures (green lines, row 5 of Table 1), compared with the reference cases of planar cells (grey lines, row 4), for perovskite layers with distinct thickness: a) 300 nm

and b) 500 nm. The inset profiles represent the total generation rate, G , along the xz cross-sectional plane of the structures. **c,d**) Profiles of the absorption density, p_{ABS} , along the same xz plane, at the wavelengths of the peaks marked by the arrows in a) and b).

Nonetheless, for the thinner 300 nm perovskite, stronger scattering is required to compensate for the reduced absorber thickness, which explains the larger R values of the thinner PSCs relative to the 500 nm ones. The optimal designs of the semi-spheroidal arrays converged to similar pitch (p) for both 300 and 500 nm perovskite, with optimal p values slightly above/below 500 nm for the superstrate/substrate configuration.

It can be seen that the substrate configuration suffers from higher parasitic absorption in most of the spectrum. At the shorter wavelengths <500 nm it is mostly attributed to the thicker 100 nm of ZnO that serves as ETL, in contrast to the 25 nm SnO₂ for the superstrate configuration. At the longer wavelengths in the NIR the high parasitic absorption occurs mainly at the rear contact, as revealed by the particularly intense hot spots present in the HTL and Au layers of these structures (see G and p_{ABS} profiles of Fig. 3), which exhibit a much higher magnitude than those of Fig. 2. The main reason for this is the fact that the HTL material (NiO_x) considered here has a considerably higher n (see Fig. S1a of SM), so the optical optimizations converged to HTL thicknesses ($t_{NiO} \sim 10-11$ nm) much lower than those (50 nm) taken for the Spiro-OMeTAD used in the superstrate PSCs.

Overall, the absolute J_{PH} values attained with optimized LT are higher in the superstrate configuration, for both 300 and 500 nm perovskite, owing to the reduced parasitic absorption. However, the photocurrent improvement relative to the planar references is slightly higher in substrate configuration, mainly because the substrate-type planar cells also suffer comparably high parasitic absorption in the UV-VIS range. For this reason, the gains with optimized LT designs in substrate PSCs are superior to those achieved with superstrate architecture.

4. Angle-resolved optical response

The dependence of the LT-enhanced PSCs performance with the incidence angle is of extreme relevance for their practical application, not only in conventional non-tracking PV installations, but specially importantly for thin-film cells integrated on bendable substrates[6,68]. In such case, the flexible solar cells will likely operate with a certain curvature, so they will be illuminated by a cone of incidence angles along their active area. As such, it is crucial to evaluate the LT performance for oblique illumination. Despite the fact that the LT designs described in the previous section were optimized for normal incidence, they maintain broadband light absorption enhancement for a wide range of incidence angles, as analyzed next.

At normal incidence, due to the spheroidal shape of the LT features, the optical response of the cells is independent of the polarization of the incident light, since the illumination is along the axis of revolution of the semi-spheroids. However, that is not the case for oblique incidence. As such, the TM (transverse magnetic) and TE (transverse electric) polarization components were computed separately, and the resulting photocurrent densities (TM J_{PH} and TE J_{PH}) are represented in Fig. 4d. The output J_{PH} for unpolarized sunlight illumination was calculated by averaging the photocurrent values obtained with the TM and TE components, and is shown in Fig. 4b,c.

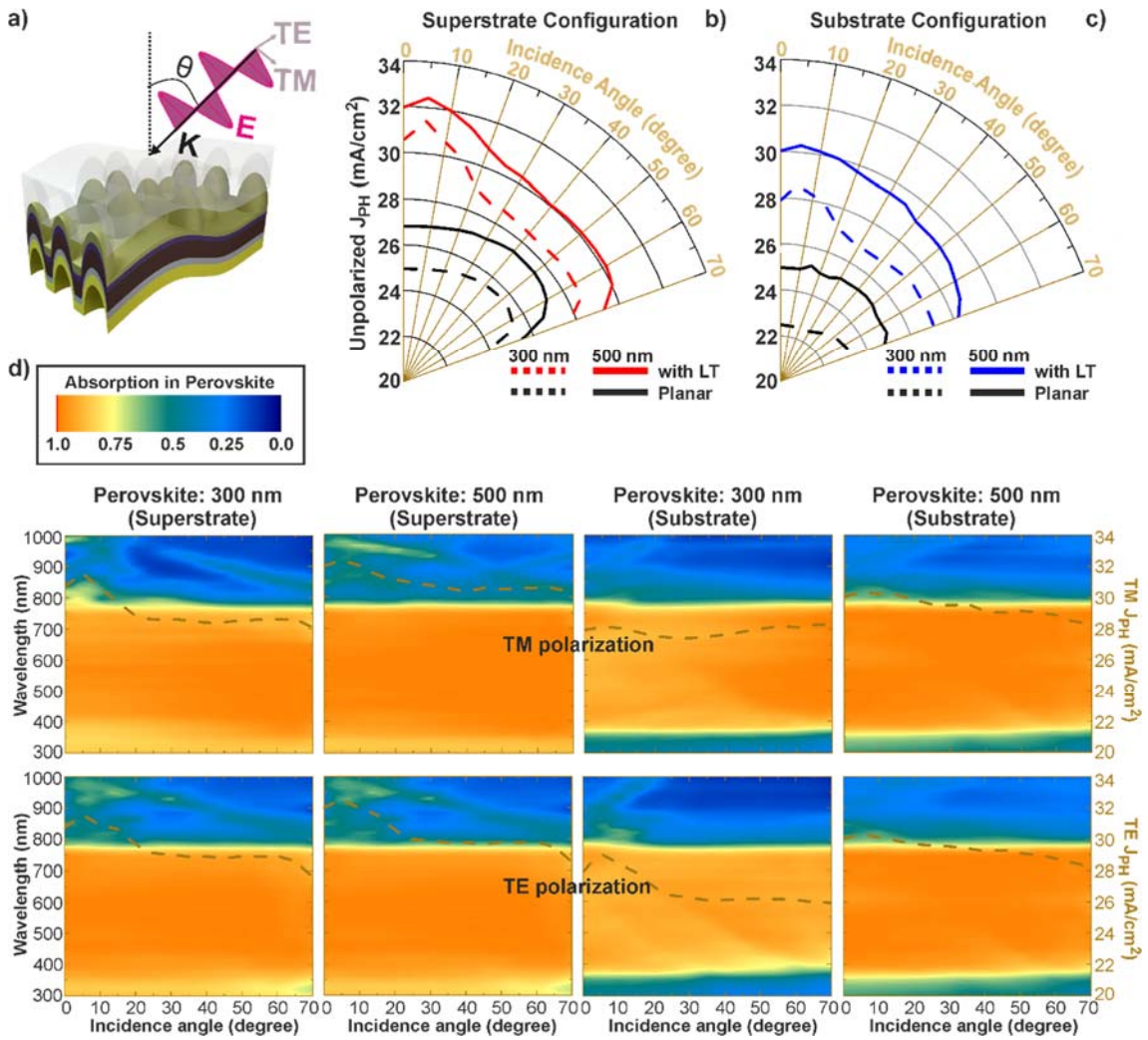


Fig. 4: **a)** Sketch of sunlight illumination of a flexible LT-enhanced PSC. **b, c)** angle-resolved unpolarized photocurrent density, J_{PH} , given by the average between the current values attained with the TM and TE polarizations, for the two solar cells configurations: superstrate (b) and substrate (c). **d)** Color plots of the absorption spectra occurring in the 300 and 500 nm PSCs, as a function of the incidence angle, for both TM (top) and TE (bottom) polarization. The dashed brown curve plotted in the graphs corresponds to the angle-resolved photocurrent density obtained for each case (values in the right axes). See Section S5 in SM for further details regarding the angular simulations of the reference planar PSCs.

In general, the planar PSCs exhibit a quite omni-directional response, particularly in the substrate configuration, since the unpolarized J_{PH} (in Fig. 4b,c) is roughly constant up to $\sim 60^\circ$ and then starts decreasing only for higher angles, as these structures do not provide scattering effects. While the unpolarized J_{PH} of the LT-enhanced PSCs generally tends to decrease with increasing angle, but the maximum reduction is only of 3-4% for the substrate configuration and of 6-7% for the superstrate configuration, for 0-60° incidence angles. Such small reduction mainly occurs due to the relatively lower absorption in the perovskite in the NIR range, as seen in Fig. 4d, as a consequence of slightly weaker scattering and waveguide mode coupling for larger angles. Nevertheless, such reduction with oblique incidence is significantly lower compared to that observed in thin-film silicon solar cells coated with optimized front LT structures[6]. This is attributed to the fact the present PSCs are conformally patterned on the photonic-structured substrates, so the corrugation of the PSC layers benefits a wider angular response with respect to LT-enhanced cells having a planar absorber. The more angle-independent J_{PH} of the substrate-type PSCs, relative to the superstrate configuration, is due to the fact that in substrate configuration the LT structures yield a higher fraction of absorption enhancement in the visible range (400-800 nm wavelengths) relative to NIR enhancement at longer wavelengths, and the gains in the visible (chiefly via anti-reflection) are less affected by the increase of the incidence angle as compared with those in the NIR (via scattering).

5. Discussion

By maximizing the broadband anti-reflection and light scattering properties of PSCs conformally deposited onto micro-structured substrates, optimized device architectures were presented with unprecedented photocurrent gains across the 300-1000 nm wavelength range of interest. Fig. 5 summarizes the predicted enhancements, along the analyzed angular range, for the two distinct perovskite thicknesses of 300 and 500 nm with superstrate and substrate cells' configurations, calculated relative to the corresponding optimized planar PSC reference cases. The gains are compared with those analytically obtained in the Lambertian cases of geometrical optics (see Table 1) at normal incidence. It should be noted that the Lambertian improvements were not calculated with respect to the same reference values of the planar PSCs, but instead relative to the same theoretical structure but without light scattering[3,5,6]. In section S6 of SM the results are compared for a distinct perovskite refractive index dispersion[59], yielding slightly lower photocurrent enhancements than those of Table 1, but a much closer propinquity to the Lambertian limits for all cases. The superstrate configuration led to higher absolute photocurrent for both perovskite thicknesses, mainly due to the thinner ETL thickness used in such architecture which yields lower parasitic absorption. Nevertheless, the substrate configuration ultimately

showed ~3-4% higher gains when compared with the corresponding planar counterpart. As expected, the highest absolute photocurrents, J_{PH} , are achieved with the 500 nm thick perovskite (32.5 and 30.2 mA/cm², respectively in superstrate and substrate configuration at normal incidence). However, the LT structures on the 300 nm perovskite yield the highest photocurrent improvements (~3-4% higher gains compared to those with 500 nm perovskite at normal incidence), as shown in Fig. 5. This matches the trend predicted from Lambertian ray optics analysis[5] - the thinner the absorber the higher the absorption enhancement that can be achieved with LT. The photocurrent gains attained with our optimized LT structures are close to those predicted by the Lambertian limits. Nevertheless, the slight differences indicate that there is still some room for further improvement of the LT scheme, for instance by tuning the refractive indices of the front (e.g. less absorbing TCO) and rear (e.g. more reflective electrode as Ag) contact layers[2,5,55].

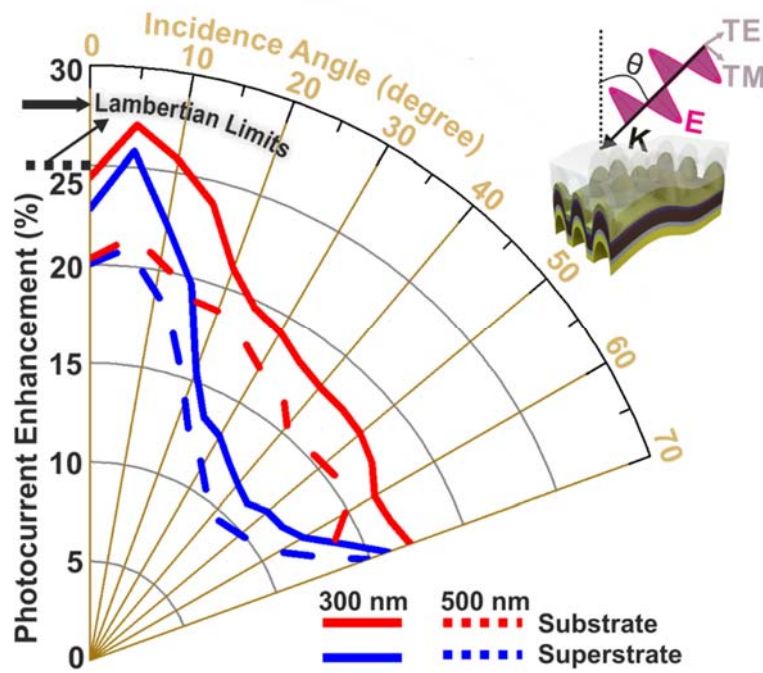


Fig. 5: Improvement in photocurrent density, J_{PH} , achieved with the optimized photonic-structured PSCs (rows of 3 and 5 of Table 1) analyzed in section 3, relative to the planar references (rows 2 and 4 of Table 1 and Sections S3 and S4), as a function of the incidence angle (θ). The Lambertian limits of LT in PSCs, in the geometrical optics regime, are also indicated for normal incidence ($\theta=0^\circ$), by the solid and dashed horizontal black lines, respectively for the 300 and 500 nm perovskite absorbers.

The substantial broadband absorption enhancement provided by the LT structures, relative to planar cells, was also demonstrated for a large range of incidence angles (0-70 degrees), as seen in Fig. 5. The gains in the substrate configuration are clearly higher than those in superstrate configuration for most of the angular range, due to the spectral differences in which the absorption

enhancements occur, as explained in section 4. It is noteworthy that the angular trends appear to be almost independent of the absorber thickness, since there is a roughly constant shift between the solid and dashed curves of Fig. 5 for the 300 and 500 nm perovskites. For all cases, the angular dependences of the photocurrent improvements are significantly higher compared to those obtained in silicon solar cells with the best-performing LT front structures[6]. This is mainly due to two reasons: first, the optimized curvature of the PSC layers in the architectures developed in this work in which the cell is conformally coated onto structured substrates; and second, the lower real part of the refractive index (see Fig. S1 in SM) of the perovskite absorber ($n \sim 2.3-2.5$) and its better index matching with the contact layers ($n \sim 1.6-2.0$) relatively to silicon-based absorbers ($n \sim 4$), which reduces parasitic absorption and reflected light escaping the cell[3,6,69]. Therefore, the optimized conformal design demonstrated in this work is preferable for flexible PSCs, as it assists their operation under bending which implies illumination from a broad angular range.

It is also important to analyze the dependency of the solar cells' response with variations in the geometrical parameters of the LT structures around the optimal values. For that, we considered the PSC design with 300 nm perovskite in the superstrate configuration (Fig. 2a), and show in Fig. 6 the variation of its absorption spectrum and resulting photocurrent with a $\pm 10\%$ deviation in the geometrical parameters (R_z , R , p). As observed in a previous work of the authors with photonic-enhanced PSCs supported of flat rear-metal contacts [5], Fig. 6a shows that the absorption in the perovskite in the shorter wavelength range (300-~450 nm) is mostly affected by variation of R_z , since the absorption in this part of the spectrum is mostly enhanced by anti-reflection effects, due to the geometrical index matching caused by the high aspect-ratio of the front structures. The influence of R_z in the absorption enhancement at the longer wavelengths is much less pronounced. Conversely, the in-plane radius, R , and array pitch, p , have a minor effect on the absorption gains in the shorter wavelengths, but have strong effect for the longer wavelengths (NIR region), as seen in Fig. 6b,c. It is observed that these two parameters have almost the same effect on the perovskite absorption gains for wavelengths above ~ 700 nm, as they both set the grating properties of the photonic structure which determine the guided-mode trapping in such NIR wavelengths. For this reason, it is observed in Fig. 6b1,c1 a higher sensitivity of the photocurrent with variation of these two parameters (determining the waveguided modes) than with variation of R_z (determining the anti-reflection). These conclusions are in line with those of a recent study demonstrating similar optical absorption enhancement effects in ultra-thin CIGS solar cells[67].

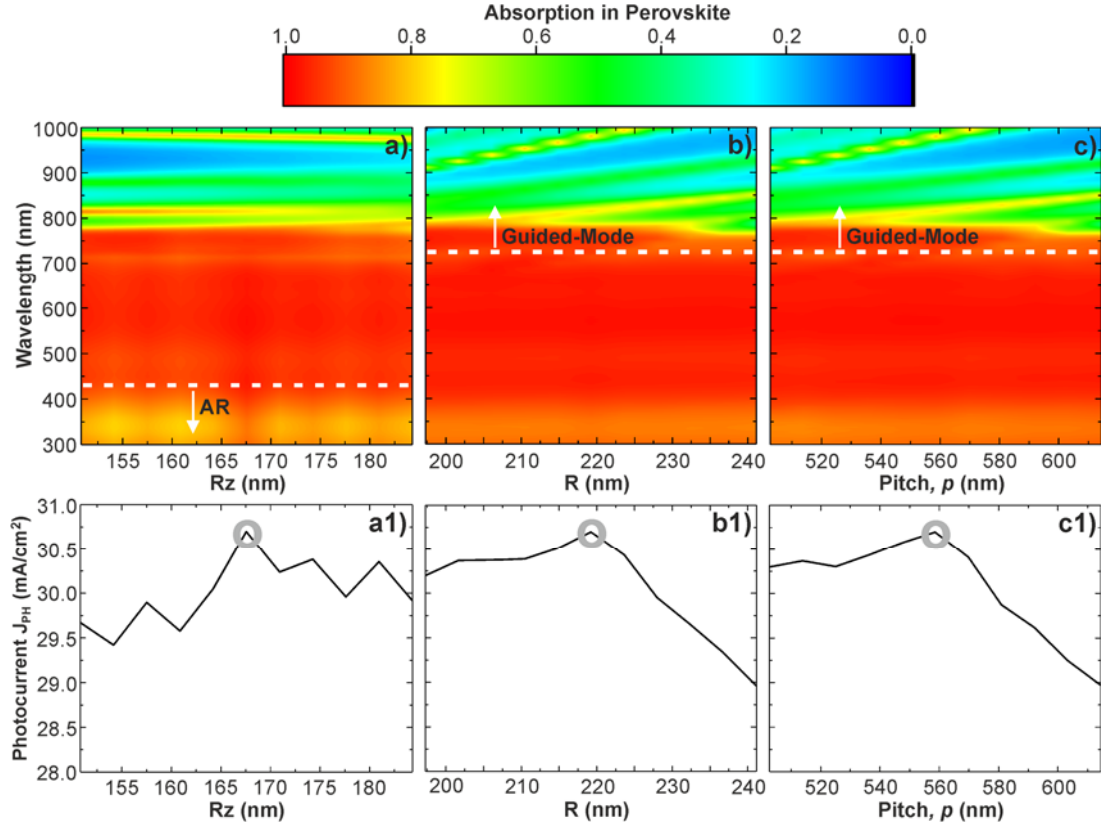


Fig. 6: Spectra of the absorption in the perovskite (top plots) and photocurrent density (J_{PH} , bottom plots) attained with a 20% variation ($\pm 10\%$ deviation) in each geometrical parameter [R_z , R and p , respectively in a), b) and c)], relative to the optimal parameter values (marked by the circles in bottom plots) for the superstrate photonic-enhanced PSC with 300 nm thick Perovskite (row 3 of Table 1, Fig. 2a).

Lastly, although outside the scope of this investigation, the rough PSC interfaces in the present LT-enhanced cell structure could raise the concern of possible electrical deterioration in practical devices fabricated with wet-coating processes. Nevertheless, the fast evolution in PSC technology has shown improved PSC deposition methods enabling conformal coating of the cell layers on micro-rough substrates and resulting in high efficiencies[70]. For instance, F. Wang et al. [71] developed a recrystallization treatment that allowed 18.6% PSC efficiency with a ~ 300 nm thick perovskite absorber conformally coated on textured glass having surface features on the order of the micrometer (as those in this study). These findings indicate that it is possible to develop non-planar PSCs without being considerably affected by the rough interfaces.

6. Conclusions

This work demonstrates the optical advantages of using photonic-structured substrates to fabricate electrically thin but optically thick solar cells, applied to perovskite PV. In the investigated light-

trapping (LT) design, the active cell materials are taken to be conformally deposited over the photonic substrates. This avoids the otherwise necessary costs associated with front-textured photonics applied to the device, as well as the deterioration of the cell layers during the implementation of such LT structures in post-processes. For instance, front-patterned TiO₂ LT coatings were proposed in a previous work and demonstrated high potential for efficiency and even UV stability improvement when integrated in the ETL of substrate-type PSCs[5]. This approach, however, requires an additional manufacturing step that can degrade the highly-sensitive PSC materials located underneath, thus posing challenges for its practical realization.

Furthermore, the present solution can be an extremely cost effective approach due to the low material usage (no extra material is used in the photonic structuring), compared to those reported in the literature[5,72], as well as being compatible with industrially-attractive processes as soft-lithography and roll-to-roll[47], since the PSCs are deposited with the established fabrication methods onto previously patterned substrates. To accommodate state-of-the-art fabrication procedures for the cells, different ETL and HTL materials were considered in the superstrate and substrate configurations[48]. Here, it is notable the resulting small thickness of the optimized ETL, HTL and TCO layers, since the optical (film-based) index-matching provides a smaller optical impact than the geometrical index-matching, thence creating a situation where smaller parasitic absorption is preferred.

We show that by carefully tuning the geometrical features on the substrates one can achieve levels of LT enhancement (up to 24.4% with 300 nm and 20.3% with 500 nm perovskite) comparable to those of the previous method[5], with the added benefit of a more omni-directional angular response (up to 70°) which is of paramount importance for flexible devices. In addition to the superior photocurrent (thus efficiency) improvements, the LT solutions designed here reveal that the perovskite thickness can be substantially reduced while maintaining high performance, as the J_{PH} values attained with the 300 nm LT-enhanced cells are considerably higher than those of the conventional 500 nm planar references (see Table 1). Such reduction in perovskite thickness from 500 to 300 nm can bring important competitive advantages: 1) an almost 2-fold reduction in the amount of the environmentally-toxic lead (Pb) compound, as well as in the material costs associated to the perovskite material (with no additional material costs for the LT structures since they are incorporated in the substrates); 2) a potential 3-fold increase in the device flexibility due to the reduced absorber thickness.

Lastly, photonic substrates as those investigated here can also be straightforwardly adapted to different types of thin-film solar cells (e.g. Si-based, CIGS, CZTS, Organic, etc.) via a fine-tuning of the geometrical parameters using a similar methodology.

Acknowledgements



This project has received funding from the European Union's Horizon 2020 research and innovation programme under the project APOLO (H2020-LCE-2017-RES-RIA), grant agreement No 763989. This publication reflects only the author's views and the European Union is not liable for any use that may be made of the information contained therein.

This work was also funded by FEDER funds, through the COMPETE 2020 Program, and national funds, through the Portuguese Foundation for Science and Technology (FCT-MCTES), under the projects UID/CTM/50025/2019 and SUPERSOLAR (PTDC/NAN-OPT/28430/2017). S. Haque acknowledges the support from FCT-MCTES through the AdvamTech PhD program scholarship PD/BD/143031/2018. M. Alexandre also acknowledges the support from FCT-MCTES through the PhD scholarship grant SFRH/BD/148078/2019.

7. References

- [1] H.A. Atwater, A. Polman, Plasmonics for improved photovoltaic devices, *Nat. Mater.* 9 (2010) 205–213. doi:10.1038/nmat2629.
- [2] V.E. Ferry, A. Polman, H.A. Atwater, Modeling Light Trapping in Nanostructured Solar Cells, *ACS Nano.* 5 (2011) 10055–10064. doi:10.1021/nn203906t.
- [3] M.J. Mendes, A. Araújo, A. Vicente, H. Águas, I. Ferreira, E. Fortunato, R. Martins, Design of optimized wave-optical spheroidal nanostructures for photonic-enhanced solar cells, *Nano Energy.* 26 (2016) 286–296. doi:10.1016/J.NANOEN.2016.05.038.
- [4] M.L. Brongersma, Y. Cui, S. Fan, Light management for photovoltaics using high-index nanostructures, *Nat. Mater.* 13 (2014) 451–460. doi:10.1038/nmat3921.
- [5] S. Haque, M.J. Mendes, O. Sanchez-Sobrado, H. Águas, E. Fortunato, R. Martins, Photonic-structured TiO₂ for high-efficiency, flexible and stable Perovskite solar cells, *Nano Energy.* 59 (2019) 91–101. doi:10.1016/J.NANOEN.2019.02.023.
- [6] M.J. Mendes, S. Haque, O. Sanchez-Sobrado, A. Araújo, H. Águas, E. Fortunato, R. Martins, Optimal-Enhanced Solar Cell Ultra-thinning with Broadband Nanophotonic Light Capture, *IScience.* 3 (2018) 238–254. doi:10.1016/j.isci.2018.04.018.
- [7] R. Schmager, G. Gomard, B.S. Richards, U.W. Paetzold, Nanophotonic perovskite layers for enhanced current generation and mitigation of lead in perovskite solar cells, *Sol.*

- Energy Mater. Sol. Cells. 192 (2019) 65–71. doi:10.1016/J.SOLMAT.2018.12.012.
- [8] A. V. Shah, H. Schade, M. Vanecek, J. Meier, E. Vallat-Sauvain, N. Wyrsh, U. Kroll, C. Droz, J. Bailat, Thin-film silicon solar cell technology, *Prog. Photovoltaics Res. Appl.* 12 (2004) 113–142. doi:10.1002/pip.533.
- [9] D.L. Staebler, C.R. Wronski, Reversible conductivity changes in discharge-produced amorphous Si, *Appl. Phys. Lett.* 31 (1977) 292–294. doi:10.1063/1.89674.
- [10] Y. Xu, T. Gong, J.N. Munday, The generalized Shockley-Queisser limit for nanostructured solar cells., *Sci. Rep.* 5 (2015) 13536. doi:10.1038/srep13536.
- [11] J. Wei, R.-P. Xu, Y.-Q. Li, C. Li, J.-D. Chen, X.-D. Zhao, Z.-Z. Xie, C.-S. Lee, W.-J. Zhang, J.-X. Tang, Enhanced Light Harvesting in Perovskite Solar Cells by a Bioinspired Nanostructured Back Electrode, *Adv. Energy Mater.* 7 (2017) 1700492. doi:10.1002/aenm.201700492.
- [12] M. Alexandre, M. Chapa, S. Haque, M.J. Mendes, H. Águas, E. Fortunato, R. Martins, Optimum Luminescent Down-Shifting Properties for High Efficiency and Stable Perovskite Solar Cells, *ACS Appl. Energy Mater.* 2 (2019) 2930–2938. doi:10.1021/acsaem.9b00271.
- [13] A. T. Vicente, A. Araújo, M.J. Mendes, D. Nunes, M.J. Oliveira, O. Sanchez-Sobrado, M.P. Ferreira, H. Águas, E. Fortunato, R. Martins, Multifunctional cellulose-paper for light harvesting and smart sensing applications, *J. Mater. Chem. C.* 6 (2018) 3143–3181. doi:10.1039/C7TC05271E.
- [14] H. Águas, T. Mateus, A. Vicente, D. Gaspar, M.J. Mendes, W.A. Schmidt, L. Pereira, E. Fortunato, R. Martins, Thin Film Silicon Photovoltaic Cells on Paper for Flexible Indoor Applications, *Adv. Funct. Mater.* 25 (2015) 3592–3598. doi:10.1002/adfm.201500636.
- [15] Q. Chen, N. De Marco, Y. (Michael) Yang, T.-B. Song, C.-C. Chen, H. Zhao, Z. Hong, H. Zhou, Y. Yang, Under the spotlight: The organic–inorganic hybrid halide perovskite for optoelectronic applications, *Nano Today.* 10 (2015) 355–396. doi:10.1016/J.NANTOD.2015.04.009.
- [16] Y. Ogomi, A. Morita, S. Tsukamoto, T. Saitho, N. Fujikawa, Q. Shen, T. Toyoda, K. Yoshino, S.S. Pandey, T. Ma, S. Hayase, $\text{CH}_3\text{NH}_3\text{Sn}_x\text{Pb}_{(1-x)}\text{I}_3$ Perovskite Solar Cells Covering up to 1060 nm, *J. Phys. Chem. Lett.* 5 (2014) 1004–1011. doi:10.1021/jz5002117.
- [17] J.H. Noh, S.H. Im, J.H. Heo, T.N. Mandal, S. Il Seok, Chemical Management for Colorful, Efficient, and Stable Inorganic–Organic Hybrid Nanostructured Solar Cells, *Nano Lett.* 13 (2013) 1764–1769. doi:10.1021/nl400349b.

- [18] C.S. Ponseca, T.J. Savenije, M. Abdellah, K. Zheng, A. Yartsev, T. Pascher, T. Harlang, P. Chabera, T. Pullerits, A. Stepanov, J.-P. Wolf, V. Sundström, Organometal Halide Perovskite Solar Cell Materials Rationalized: Ultrafast Charge Generation, High and Microsecond-Long Balanced Mobilities, and Slow Recombination, *J. Am. Chem. Soc.* 136 (2014) 5189–5192. doi:10.1021/ja412583t.
- [19] H. Oga, A. Saeki, Y. Ogomi, S. Hayase, S. Seki, Improved Understanding of the Electronic and Energetic Landscapes of Perovskite Solar Cells: High Local Charge Carrier Mobility, Reduced Recombination, and Extremely Shallow Traps, *J. Am. Chem. Soc.* 136 (2014) 13818–13825. doi:10.1021/ja506936f.
- [20] F. Huang, M. Li, P. Siffalovic, G. Cao, J. Tian, From scalable solution fabrication of perovskite films towards commercialization of solar cells, *Energy Environ. Sci.* 12 (2019) 518–549. doi:10.1039/C8EE03025A.
- [21] A. Kojima, K. Teshima, Y. Shirai, T. Miyasaka, Organometal Halide Perovskites as Visible-Light Sensitizers for Photovoltaic Cells, *J. Am. Chem. Soc.* 131 (2009) 6050–6051. doi:10.1021/ja809598r.
- [22] M. Saliba, T. Matsui, J.-Y. Seo, K. Domanski, J.-P. Correa-Baena, M.K. Nazeeruddin, S.M. Zakeeruddin, W. Tress, A. Abate, A. Hagfeldt, M. Grätzel, Cesium-containing triple cation perovskite solar cells: improved stability, reproducibility and high efficiency, *Energy Environ. Sci.* 9 (2016) 1989–1997. doi:10.1039/C5EE03874J.
- [23] D. Bi, C. Yi, J. Luo, J.-D. Décoppet, F. Zhang, S.M. Zakeeruddin, X. Li, A. Hagfeldt, M. Grätzel, Polymer-templated nucleation and crystal growth of perovskite films for solar cells with efficiency greater than 21%, *Nat. Energy.* 1 (2016) 16142. doi:10.1038/nenergy.2016.142.
- [24] W.S. Yang, B.-W. Park, E.H. Jung, N.J. Jeon, Y.C. Kim, D.U. Lee, S.S. Shin, J. Seo, E.K. Kim, J.H. Noh, S. Il Seok, Iodide management in formamidinium-lead-halide-based perovskite layers for efficient solar cells., *Science.* 356 (2017) 1376–1379. doi:10.1126/science.aan2301.
- [25] Y. Cheng, F. So, S.-W. Tsang, Progress in air-processed perovskite solar cells: from crystallization to photovoltaic performance, *Mater. Horizons.* (2019). doi:10.1039/C9MH00325H.
- [26] Best Research-Cell Efficiency Chart | Photovoltaic Research | NREL, (n.d.). <https://www.nrel.gov/pv/cell-efficiency.html> (accessed September 9, 2019).
- [27] J. Burschka, N. Pellet, S.-J. Moon, R. Humphry-Baker, P. Gao, M.K. Nazeeruddin, M. Grätzel, Sequential deposition as a route to high-performance perovskite-sensitized solar

- cells, *Nature*. 499 (2013) 316–319. doi:10.1038/nature12340.
- [28] W. Nie, H. Tsai, R. Asadpour, J.-C. Blancon, A.J. Neukirch, G. Gupta, J.J. Crochet, M. Chhowalla, S. Tretiak, M.A. Alam, H.-L. Wang, A.D. Mohite, High-efficiency solution-processed perovskite solar cells with millimeter-scale grains, *Science* (80-.). 347 (2015) 522–525. doi:10.1126/SCIENCE.AAA0472.
- [29] N. Arora, M.I. Dar, A. Hinderhofer, N. Pellet, F. Schreiber, S.M. Zakeeruddin, M. Grätzel, Perovskite solar cells with CuSCN hole extraction layers yield stabilized efficiencies greater than 20%, *Science* (80-.). 358 (2017) 768–771. doi:10.1126/SCIENCE.AAM5655.
- [30] T.M. Brenner, D.A. Egger, L. Kronik, G. Hodes, D. Cahen, Hybrid organic—inorganic perovskites: low-cost semiconductors with intriguing charge-transport properties, *Nat. Rev. Mater.* 1 (2016) 15007. doi:10.1038/natrevmats.2015.7.
- [31] O. Sanchez-Sobrado, M.J. Mendes, S. Haque, T. Mateus, H. Aguas, E. Fortunato, R. Martins, Lightwave trapping in thin film solar cells with improved photonic-structured front contacts, *J. Mater. Chem. C*. 7 (2019) 6456–6464. doi:10.1039/C8TC06092D.
- [32] A. Peer, R. Biswas, J.-M. Park, R. Shinar, J. Shinar, Light management in perovskite solar cells and organic LEDs with microlens arrays, *Opt. Express*. 25 (2017) 10704. doi:10.1364/OE.25.010704.
- [33] H. Wang, B. Cai, X. Yuan, Significant light absorption improvement in perovskite/CIGS tandem solar cells with dielectric nanocone structures, *J. Phys. Conf. Ser.* 844 (2017) 012004. doi:10.1088/1742-6596/844/1/012004.
- [34] N. Horiuchi, Photonic nanojets, *Nat. Photonics*. 6 (2012) 138–139. doi:10.1038/nphoton.2012.43.
- [35] B. Dudem, J.H. Heo, J.W. Leem, J.S. Yu, S.H. Im, CH₃NH₃PbI₃ planar perovskite solar cells with antireflection and self-cleaning function layers, *J. Mater. Chem. A*. 4 (2016) 7573–7579. doi:10.1039/C6TA01800A.
- [36] T.K. Nguyen, P.T. Dang, K.Q. Le, Numerical design of thin perovskite solar cell with fiber array-based anti-reflection front electrode for light-trapping enhancement, *J. Opt.* 18 (2016) 125901. doi:10.1088/2040-8978/18/12/125901.
- [37] U.W. Paetzold, W. Qiu, F. Finger, J. Poortmans, D. Cheyng, Nanophotonic front electrodes for perovskite solar cells, *Appl. Phys. Lett.* 106 (2015) 173101. doi:10.1063/1.4918751.
- [38] S.M. Kang, S. Jang, J.-K. Lee, J. Yoon, D.-E. Yoo, J.-W. Lee, M. Choi, N.-G. Park, Moth-

- Eye TiO₂ Layer for Improving Light Harvesting Efficiency in Perovskite Solar Cells, *Small*. 12 (2016) 2443–2449. doi:10.1002/smll.201600428.
- [39] S.-J. Ha, J.H. Heo, S.H. Im, J.H. Moon, Mesoscopic CH₃NH₃PbI₃ perovskite solar cells using TiO₂ inverse opal electron-conducting scaffolds, *J. Mater. Chem. A*. 5 (2017) 1972–1977. doi:10.1039/C6TA07004C.
- [40] Y. Luo, S. Liu, N. Barange, L. Wang, F. So, Perovskite Solar Cells on Corrugated Substrates with Enhanced Efficiency, *Small*. 12 (2016) 6346–6352. doi:10.1002/smll.201601974.
- [41] J. Werner, F. Sahli, F. Fu, J.J. Diaz Leon, A. Walter, B.A. Kamino, B. Niesen, S. Nicolay, Q. Jeangros, C. Ballif, Perovskite/Perovskite/Silicon Monolithic Triple-Junction Solar Cells with a Fully Textured Design, *ACS Energy Lett.* 3 (2018) 2052–2058. doi:10.1021/acsenerylett.8b01165.
- [42] D. Chen, P. Manley, P. Tockhorn, D. Eisenhauer, G. Köppel, M. Hammerschmidt, S. Burger, S. Albrecht, C. Becker, K. Jäger, Nanophotonic light management for perovskite–silicon tandem solar cells, *J. Photonics Energy*. 8 (2018) 1. doi:10.1117/1.JPE.8.022601.
- [43] M.I. Hossain, W. Qarony, V. Jovanov, Y.H. Tsang, D. Knipp, Nanophotonic design of perovskite/silicon tandem solar cells, *J. Mater. Chem. A*. 6 (2018) 3625–3633. doi:10.1039/C8TA00628H.
- [44] J. Hao, H. Hao, J. Li, L. Shi, T. Zhong, C. Zhang, J. Dong, J. Xing, H. Liu, Z. Zhang, Light Trapping Effect in Perovskite Solar Cells by the Addition of Ag Nanoparticles, Using Textured Substrates., *Nanomater. (Basel, Switzerland)*. 8 (2018). doi:10.3390/nano8100815.
- [45] R.T. Ginting, S. Kaur, D.-K. Lim, J.-M. Kim, J.H. Lee, S.H. Lee, J.-W. Kang, Plasmonic Effect of Gold Nanostars in Highly Efficient Organic and Perovskite Solar Cells, *ACS Appl. Mater. Interfaces*. 9 (2017) 36111–36118. doi:10.1021/acсами.7b11084.
- [46] M. Long, Z. Chen, T. Zhang, Y. Xiao, X. Zeng, J. Chen, K. Yan, J. Xu, Ultrathin efficient perovskite solar cells employing a periodic structure of a composite hole conductor for elevated plasmonic light harvesting and hole collection, *Nanoscale*. 8 (2016) 6290–6299. doi:10.1039/C5NR05042A.
- [47] O. Sanchez-Sobrado, M.J. Mendes, S. Haque, T. Mateus, A. Araujo, H. Aguas, E. Fortunato, R. Martins, Colloidal-lithographed TiO₂ photonic nanostructures for solar cell light trapping, *J. Mater. Chem. C*. 5 (2017) 6852–6861. doi:10.1039/C7TC01756A.
- [48] D. Yang, R. Yang, S. Priya, S.F. Liu, Recent Advances in Flexible Perovskite Solar Cells: Fabrication and Applications, *Angew. Chemie Int. Ed.* 58 (2019) 4466–4483.

doi:10.1002/anie.201809781.

- [49] P.M.P. Salomé, B. Vermang, R. Ribeiro-Andrade, J.P. Teixeira, J.M. V. Cunha, M.J. Mendes, S. Haque, J. Borme, H. Águas, E. Fortunato, R. Martins, J.C. González, J.P. Leitão, P.A. Fernandes, M. Edoff, S. Sadewasser, Passivation of Interfaces in Thin Film Solar Cells: Understanding the Effects of a Nanostructured Rear Point Contact Layer, *Adv. Mater. Interfaces*. 5 (2018) 1701101. doi:10.1002/admi.201701101.
- [50] F. Neves, A. Stark, N. Schell, M.J. Mendes, H. Aguas, E. Fortunato, R. Martins, J.B. Correia, A. Joyce, Investigation of single phase $Cu_2ZnS_{n-x}Sb_{1-x}S_4$ compounds processed by mechanochemical synthesis, *Phys. Rev. Mater.* 2 (2018) 075404. doi:10.1103/PhysRevMaterials.2.075404.
- [51] M. Chapa, M.F. Alexandre, M.J. Mendes, H. Águas, E. Fortunato, R. Martins, All-Thin-Film Perovskite/C–Si Four-Terminal Tandems: Interlayer and Intermediate Contacts Optimization, *ACS Appl. Energy Mater.* 2 (2019) 3979–3985. doi:10.1021/acsaem.9b00354.
- [52] F. Fu, T. Feurer, T.P. Weiss, S. Pisoni, E. Avancini, C. Andres, S. Buecheler, A.N. Tiwari, High-efficiency inverted semi-transparent planar perovskite solar cells in substrate configuration, *Nat. Energy*. 2 (2016) 16190. doi:10.1038/nenergy.2016.190.
- [53] L. Qiu, J. Deng, X. Lu, Z. Yang, H. Peng, Integrating Perovskite Solar Cells into a Flexible Fiber, *Angew. Chemie Int. Ed.* 53 (2014) 10425–10428. doi:10.1002/anie.201404973.
- [54] M. Jošt, S. Albrecht, L. Kegelmann, C.M. Wolff, F. Lang, B. Lipovšek, J. Krč, L. Korte, D. Neher, B. Rech, M. Topič, Efficient Light Management by Textured Nanoimprinted Layers for Perovskite Solar Cells, *ACS Photonics*. 4 (2017) 1232–1239. doi:10.1021/acsp Photonics.7b00138.
- [55] V.E. Ferry, M.A. Verschuuren, M.C. van Lare, R.E.I. Schropp, H.A. Atwater, A. Polman, Optimized Spatial Correlations for Broadband Light Trapping Nanopatterns in High Efficiency Ultrathin Film a-Si:H Solar Cells, *Nano Lett.* 11 (2011) 4239–4245. doi:10.1021/nl202226r.
- [56] M.G. Deceglie, V.E. Ferry, A.P. Alivisatos, H.A. Atwater, Design of Nanostructured Solar Cells Using Coupled Optical and Electrical Modeling, *Nano Lett.* 12 (2012) 2894–2900. doi:10.1021/nl300483y.
- [57] L.J. Phillips, A.M. Rashed, R.E. Treharne, J. Kay, P. Yates, I.Z. Mitrovic, A. Weerakkody, S. Hall, K. Durose, Dispersion relation data for methylammonium lead triiodide perovskite deposited on a (100) silicon wafer using a two-step vapour-phase reaction process, *Data Br.* 5 (2015) 926–928. doi:10.1016/J.DIB.2015.10.026.

- [58] Refractive index database, (n.d.). <https://refractiveindex.info/> (accessed June 1, 2019).
- [59] M. van Eerden, M. Jaysankar, A. Hadipour, T. Merckx, J.J. Schermer, T. Aernouts, J. Poortmans, U.W. Paetzold, Optical Analysis of Planar Multicrystalline Perovskite Solar Cells, *Adv. Opt. Mater.* 5 (2017) 1700151. doi:10.1002/adom.201700151.
- [60] FDTD Solutions | Lumerical's Nanophotonic FDTD Simulation Software, (n.d.). <https://www.lumerical.com/tcad-products/fdtd/> (accessed March 7, 2018).
- [61] M.J. Mendes, H.K. Schmidt, M. Pasquali, Brownian Dynamics Simulations of Single-Wall Carbon Nanotube Separation by Type Using Dielectrophoresis, *J. Phys. Chem. B.* 112 (2008) 7467–7477. doi:10.1021/jp711450w.
- [62] Q. Jiang, X. Zhang, J. You, SnO₂: A Wonderful Electron Transport Layer for Perovskite Solar Cells, *Small.* 14 (2018) 1801154. doi:10.1002/smll.201801154.
- [63] P. Zhang, J. Wu, T. Zhang, Y. Wang, D. Liu, H. Chen, L. Ji, C. Liu, W. Ahmad, Z.D. Chen, S. Li, Perovskite Solar Cells with ZnO Electron-Transporting Materials, *Adv. Mater.* 30 (2018) 1703737. doi:10.1002/adma.201703737.
- [64] A. Al Mamun, T.T. Ava, T.M. Abdel-Fattah, H.J. Jeong, M.S. Jeong, S. Han, H. Yoon, G. Namkoong, Effect of hot-casted NiO hole transport layer on the performance of perovskite solar cells, *Sol. Energy.* 188 (2019) 609–618. doi:10.1016/J.SOLENER.2019.06.040.
- [65] G.-W. Kim, D. V. Shinde, T. Park, Thickness of the hole transport layer in perovskite solar cells: performance versus reproducibility, *RSC Adv.* 5 (2015) 99356–99360. doi:10.1039/C5RA18648J.
- [66] D. Liu, T.L. Kelly, Perovskite solar cells with a planar heterojunction structure prepared using room-temperature solution processing techniques, *Nat. Photonics.* 8 (2014) 133–138. doi:10.1038/nphoton.2013.342.
- [67] H.-L. Chen, A. Cattoni, R. De Lépinau, A.W. Walker, O. Höhn, D. Lackner, G. Siefer, M. Faustini, N. Vandamme, J. Goffard, B. Behaghel, C. Dupuis, N. Bardou, F. Dimroth, S. Collin, A 19.9%-efficient ultrathin solar cell based on a 205-nm-thick GaAs absorber and a silver nanostructured back mirror, *Nat. Energy.* 4 (2019) 761–767. doi:10.1038/s41560-019-0434-y.
- [68] P. Spinelli, M.A. Verschuuren, A. Polman, Broadband omnidirectional antireflection coating based on subwavelength surface Mie resonators, *Nat. Commun.* 3 (2012) 692. doi:10.1038/ncomms1691.
- [69] W. Qarony, M.I. Hossain, A. Salleo, D. Knipp, Y.H. Tsang, Rough versus planar interfaces: How to maximize the short circuit current of perovskite single and tandem solar

- cells, *Mater. Today Energy*. 11 (2019) 106–113. doi:10.1016/J.MTENER.2018.10.001.
- [70] S.A. Lukas Kegelmann, Philipp Tockhorn, Max Grischek, José A. Márquez, Thomas Unold, Wilfried Lövenich, Dieter Neher, SpiDOT: mixtures of undoped Spiro-OMeTAD and PEDOT to reduce charge recombination and absorption losses in monolithic perovskite/silicon tandem solar cells, in: *Proc. Int. Conf. Hybrid Org. Photovoltaics*, n.d. <https://www.nanoge.org/proceedings/HOPV19/5c530c600044c8385969dadb>.
- [71] F. Wang, Y. Zhang, M. Yang, L. Fan, L. Yang, Y. Sui, J. Yang, X. Zhang, Toward ultra-thin and omnidirectional perovskite solar cells: Concurrent improvement in conversion efficiency by employing light-trapping and recrystallizing treatment, *Nano Energy*. 60 (2019) 198–204. doi:10.1016/j.nanoen.2019.03.059.
- [72] H. Zhang, J. Toudert, Optical management for efficiency enhancement in hybrid organic-inorganic lead halide perovskite solar cells, *Sci. Technol. Adv. Mater.* 19 (2018) 411–424. doi:10.1080/14686996.2018.1458578.